Electrochemical Fabrication of Strontium-Doped TiO 2 Nanotube Array Electrodes and Investigation of Their Photoelectrochemical Properties

ARTICLE *in* THE JOURNAL OF PHYSICAL CHEMISTRY C · JULY 2011

Impact Factor: 4.77

4 AUTHORS:

Hoda Amani Hamedani
Georgia Institute of Technology
16 PUBLICATIONS **115** CITATIONS
SEE PROFILE

Nageh K. Allam
Massachusetts Institute of Technology
96 PUBLICATIONS **1,757** CITATIONS
SEE PROFILE

Hamid Garmestani
Georgia Institute of Technology
186 PUBLICATIONS **2,490** CITATIONS
SEE PROFILE

Mostafa A El-Sayed
Georgia Institute of Technology
676 PUBLICATIONS **55,526** CITATIONS
SEE PROFILE

THE JOURNAL OF PHYSICAL CHEMISTRY C

ARTICLE

pubs.acs.org/JPCC

Electrochemical Fabrication of Strontium-Doped TiO_2 Nanotube Array Electrodes and Investigation of Their Photoelectrochemical Properties

Hoda A. Hamedani,[†] Nageh K. Allam,[*,§] Hamid Garmestani,[†] and Mostafa A. El-Sayed[*,‡]

[†]School of Materials Science and Engineering, [‡]Laser Dynamics Laboratory, School of Chemistry and Biochemistry, Georgia Institute of Technology, Atlanta, Georgia 30332, United States

[§]Department of Electrical Engineering and Computer Science, Massachusetts Institute of Technology, Cambridge, Massachusetts 02139, United States

ABSTRACT: In recent years, considerable efforts have been made to improve the performance of photoactive nanostructured materials for water-splitting applications. Herein, we report on the fabrication and photoelectrochemical properties of highly ordered Sr-doped TiO_2 nanotube arrays synthesized via a one-step electrochemical anodization technique. Nanotube arrays of Sr-doped TiO_2 were synthesized via anodization of titanium foil in aqueous electrolytes containing NH_4F and various concentrations of $Sr(OH)_2$ at different electrolyte pHs. The morphology and quality of the fabricated materials were found to be significantly affected by the pH of the electrolyte as well as the solubility limit of $Sr(OH)_2$ in the test electrolyte. The photoelectrochemical measurements revealed that Sr doping can significantly improve the photoconversion efficiency of the material. Using Sr-doped TiO_2 nanotube arrays, an electrode photoconversion efficiency of 0.69% was obtained, which is more than 3 times higher than that of the undoped nanotube arrays (0.2%) fabricated and tested under the same conditions.

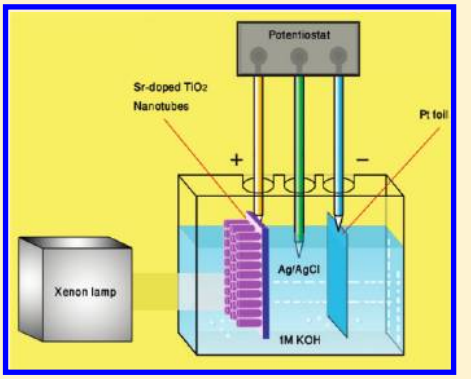

INTRODUCTION

Because of the world's ever increasing consumption of fossil fuels and its inevitable environmental impacts, extensive research efforts have been recently focused on the development of clean and more viable forms of renewable energy. One of the most promising alternative energy carriers, though available in limited quantity in nature, is hydrogen gas, which is environmentally friendly and has a high energy content.[1] With the revolution of nanotechnology, it is now generally recognized that the nanoscale control of metal oxide architectures permits significant enhancement of their performance in various applications. Therefore, in recent years, considerable efforts have been made to improve the performance of photoactive nanostructured materials for a plethora of applications.[2] In particular, TiO_2 nanotube arrays formed by anodization[3−10] have recently been extensively studied and employed in many applications. Properties, such as low cost, nontoxicity, vectorial charge transfer, and very high photocorrosion resistance compared with that of other metal oxides, make TiO_2 an interesting candidate for a plethora of applications.[11] However, the relatively low efficiency of light utilization due to the wide band gap (3.0−3.2 eV) of the material limits its use in those applications based on the photocatalytic activity.

In photoelectrochemical water splitting, although the band gap of the photocatalyst must be large enough (>1.23 eV) to dissociate water into hydrogen and oxygen (the conduction band is more negative than the reduction potential of H^+/H_2, whereas the valence band is more positive than the oxidation potential of O_2/H_2O),[12] it should be low enough to ensure the absorption of enough light for efficient device performance. More efficient visible light utilization would render this titania system quite attractive for water splitting with sunlight as the energy source. Recent and very active research relates to doping the wide-band-gap semiconducting metal oxides with cations and anions, rendering these oxides sensitive to visible light. In this regard, enhancement in the visible light photoactivity of TiO_2 has been studied by introducing a wide range of transition metals, including Fe, Mo, Mg, Ag, Pt, Co, Cr, and Mn,[4,13,14] and nonmetal elements, such as N, C, and B,[15−17] in the form of dopants or lower-band-gap oxide composites with TiO_2.[16] Of particular interest, strontium titanate ($SrTiO_3$) has been intensively investigated as a photoanode for water splitting due to its high corrosion resistance, excellent photocatalytic activity, high stability, and nontoxicity.[18−20] Although $SrTiO_3$ has band edges that straddle both oxygen and hydrogen redox potentials, it still suffers from its wide-band-gap (3.2 eV) nature. Recently, the specific phenomenon of combining the properties of both titania and $SrTiO_3$ has attracted great attention.[21−23] Jitputti and co-workers reported the hydrothermal synthesis of $SrTiO_3$ from amorphous TiO_2 nanotube arrays.[24]

Received: February 4, 2011
Revised: May 6, 2011
Published: June 10, 2011

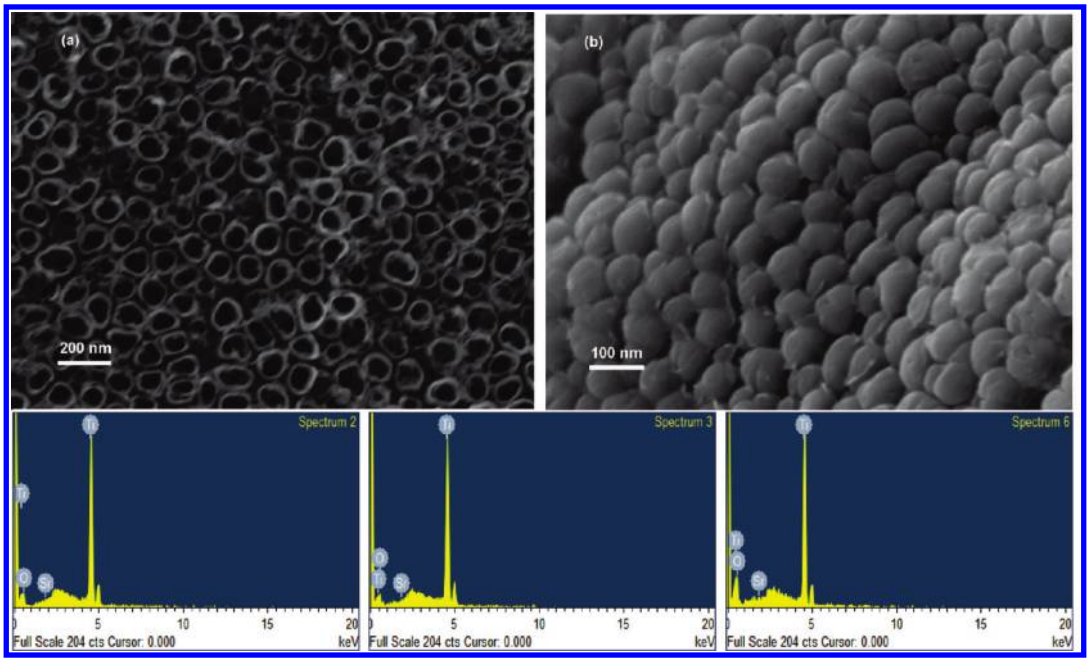

Figure 1. FESEM (a) top-view and (b) bottom-view images of the anodically fabricated Sr-doped TiO_2 nanotubes along with the corresponding EDS results at different locations on the nanotubes' surface.

Using the same hydrothermal post-treatment method, Kamat and co-workers were able to fabricate TiO_2 nanotubes decorated with $SrTiO_3$ particles/clusters. The resulting composite material ($SrTiO_3/TiO_2$) showed improved photoelectrochemical performance compared with pure TiO_2 only when $SrTiO_3$ nanocrystallites were well-dispersed on the TiO_2 nanotube walls.[21] However, a more controlled protocol is still needed to get the full benefit of the material. Also, the high temperature needed during the hydrothermal processing results in the lack of control of the structural features of the material. Considering the advantages of doping and decoration approaches on the improvement of the band gap of the material, it would be more desirable to incorporate metal ions into the TiO_2 nanotube arrays during their fabrication. Therefore, in situ band-gap engineering of the TiO_2 nanotubes seems to be a promising alternative strategy to decrease such structural imperfections and morphological defects imposed by multistep fabrication methods.

Herein, we report on the room-temperature in situ doping of TiO_2 nanotube arrays with Sr ions during their fabrication. The effect of two processing parameters, dopant concentration and electrolyte pH, on the morphological and structural properties of the material is investigated. We were able to obtain Sr-doped nanotube arrays in the crystalline form (after annealing) while maintaining the vertical alignment of the nanotube arrays. The resulting nanotube arrays showed a significant enhancement in their photoelectrochemical properties compared with pure (undoped) nanotubes fabricated and tested under the same conditions.

EXPERIMENTAL SECTION

Preparation of Sr-Doped TiO_2 Nanotube Arrays. Prior to anodization, pure titanium foil samples (Alfa Aesar, 99.9+%) were ultrasonically cleaned with acetone, followed by a deionized water rinse. The anodization was performed in a two-electrode electrochemical cell, with the titanium foil as the working electrode and platinum foil as the counter electrode, at room temperature (approximately 22 °C). Samples were anodized in electrolytes containing 0.2 M NH_4F (Alfa Aesar, 98% min.) mixed with 0.02, 0.04, or 0.06 M anhydrous strontium hydroxide ($Sr(OH)_2$) salt (Pfaltz and Bauer Inc., 99%) at 20 V for 3 h. The pH of the electrolyte was controlled by the addition of 0.1 M H_3PO_4 (J.T. Baker, ACS grade, 85.0−87.0%) to the solution. After anodization, the samples were rinsed thoroughly with deionized water and isopropyl alcohol, then dried under a stream of nitrogen. Subsequently, samples were crystallized by oxygen annealing at 450 °C for 4 h with a heating and cooling rate of 1 °C/min.

Morphological and Structural Characterization. The morphology and composition of the Sr-doped TiO_2 nanotubes were examined using a field emission scanning electron microscope (FESEM-Zeiss SEM Ultra60) equipped with an EDS (energy-dispersive X-ray spectroscopy) detector. The crystal structure was determined via glancing angle X-ray diffraction (GAXRD) using an X'Pert PRO MRD diffractometer with a Cu Kα radiation source. The surface properties and composition of the samples were analyzed by X-ray photoelectron spectroscopy using a Thermo Scientific K-Alpha XPS with an Al anode. Photoelectrons were collected in a hybrid mode over an analysis area of about 1.5 mm^2 by charge referencing the spectra to O 1s at 532 eV. Light absorption properties were performed using a Shimadzu UV-3101PC UV−vis-NIR spectrophotometer with a wavelength range of 300−800 nm.

Photoelectrochemical Measurements. The photoelectrochemical properties were investigated in 1.0 M KOH solution using a three-electrode configuration with Sr-doped nanotube array photoanodes, saturated Ag/AgCl as a reference electrode, and platinum foil as a counter electrode. A scanning potentiostat (CH Instruments, model CH 660D) was used to measure dark

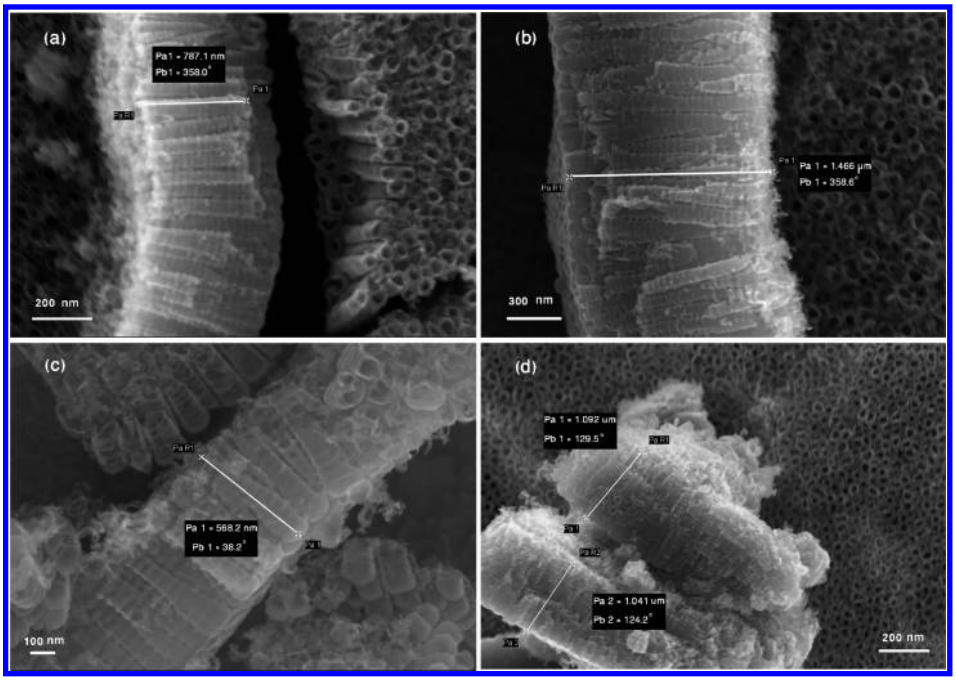

Figure 2. FESEM cross-sectional views of the anodically fabricated Sr-doped TiO_2 nanotubes for (a) 0.02 M at pH = 2, (b) 0.02 M at pH = 3, (c) 0.04 M at pH = 2, and (d) 0.04 M at pH = 3.

and illuminated currents at a scan rate of 10 mV/s. Sunlight was simulated with a 300 W xenon ozone-free lamp (Spectra Physics) and AM 1.5 G filter at 100 mW/cm^2

RESULTS AND DISCUSSION

Figure 1a shows a typical field emission scanning electron microscopy (FESEM) top-view image of the fabricated TiO_2 nanotubes in an electrolyte containing 0.02 M $Sr(OH)_2$. It can be seen that the nanotubes are open at the top end with an average diameter of approximately 100 nm, which indicates that the Sr doping does not destroy the tubular structure. The closed bottom seen in Figure 1b corresponds to the barrier layer, similar to the case of pore formation of Al.[25] The energy-dispersive X-ray spectroscopy (EDS) analysis confirms that the fabricated nanotubes are composed of Sr, Ti, and O, confirming the doping of Sr into TiO_2. Note that the EDS spectra were taken over different spots on the nanotube surface with very reproducible peaks obtained, especially those related to Sr. It is noteworthy to mention that, irrespective of the $Sr(OH)_2$ concentration, the resulting Sr-doped nanotubes were identical in terms of morphology, especially the tube diameters (100 ± 10 nm). Note that the use of $Sr(OH)_2$ in a concentration close to its solubility limit in water (1.77 g/100 mL at 20 °C)[26] results in the formation of heavy precipitates on the nanotube surface.

However, cross-sectional characterization of the fabricated Sr-doped TiO_2 nanotubes revealed that the nanotube length is a function of the electrolyte pH. This effect is shown in Figure 2. Note that the length of the Sr-doped nanotubes changes from about 0.7 to 1.4 μm in 0.02 M dopant concentration by changing the electrolyte pH from 2 to 3 (Figure 2a,b). The same effect was seen in electrolytes containing 0.04 and 0.06 M at pH 2 to 3; see Figure 2c,d. This effect shows that increasing the pH of the electrolyte from 2 to 3 resulted in doubling the nanotube length, which can be considered as one of the determinant factors in the preparation of doped nanotube arrays. Grimes and co-workers observed the same trend upon the fabrication of undoped titania nanotube arrays where longer nanotubes formed in higher pH solutions.[11]

Figure 3 shows the GAXRD patterns of the annealed pure and Sr-doped TiO_2 nanotube arrays prepared in electrolytes of pH 3. All patterns confirm the crystalline nature of the electrodes with reflections mainly from TiO_2 (anatase phase). Additionally, weak peaks of $SrTiO_3$ are also observed in Sr-doped samples that can be associated with partial formation of $SrTiO_3$ with the growth of (100), (110), (111), and (200) planes of $SrTiO_3$ corresponding to the peak indexed at 23, 34, 40, and 48°, respectively (PDF card 35-734, JCPDS).[27,28] Note the shift in the anatase peak (101) in all doped samples compared to the undoped one. This shift can be attributed to the incorporation of the Sr^{2+} with a larger ionic radius (1.32 Å) than that of Ti^{4+} (0.75 Å) into the crystal lattice of TiO_2.[29] As the concentration of the dopant increases, more Sr^{2+} ions are incorporated into the TiO_2 crystal lattice, and as a result, the corresponding peaks are more shifted to the lower angle side. For example, the anatase (101) for pure TiO_2 appears at 2θ = 25.8°, whereas that for the Sr-doped TiO_2 (0.02 M) appears at 2θ = 25.01°. In addition, the increase in peak intensity relative to the dopant concentration may indicate that the crystallinity is slightly decreased with increasing Sr dopant concentration; this effect may be related to the random substitution of the large Sr^{2+} ions in the TiO_2 lattice that cause structural strain and disorder in the TiO_2 crystalline lattice structure.[30] Note that only reflections for the anatase polymorph of titania was detected, which added to the value of the fabricated electrodes as anatase is the most photoactive polymorph of titania. Also, the conduction band edge of $SrTiO_3$ is about 200 mV more negative than that of TiO_2,[31] which makes $SrTiO_3$ a good candidate for coupling with TiO_2 and is expected to improve

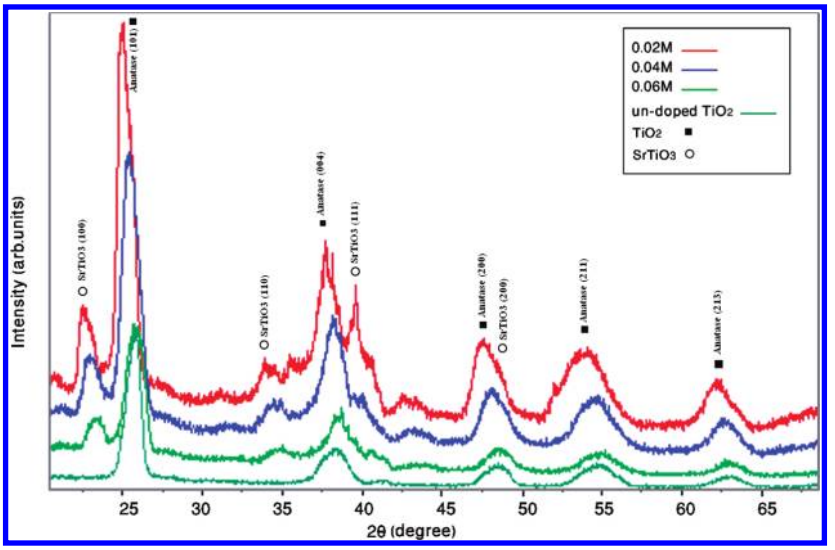

Figure 3. Glancing angle X-ray diffraction patterns of pure and Sr-doped TiO_2 nanotube samples obtained at different Sr-dopant concentrations and electrolyte pH = 3.

the overall photoelectrochemical performance of the fabricated electrodes.

To further investigate the composition of the fabricated electrodes, X-ray photoelectron spectroscopy (XPS) analysis was performed on the as-prepared nanotube arrays. Figure 4 shows the XPS results as a function of dopant concentration for a set of samples synthesized in a pH 2 electrolyte.

Figure 4a shows Ti 2p spectra with two peaks obtained corresponding to Ti $2p_{3/2}$ and Ti $2p_{1/2}$ photoemission spectra with a spin−orbit splitting of 5.7 eV, confirming that both signals correspond to Ti^{4+}.[10] Figure 4b shows O 1s photoemission spectra at 531 eV, which can be associated with the existence of metal oxides. Figure 4c shows the Sr 3d core-level XPS spectra. Increasing the dopant concentration leads to a shift toward the lower binding energy. This can be explained on the basis of the electronegativity of strontium (0.95) being lower than that of Ti (1.54) on the Pauling scale. The O 1s and Ti 2p peaks with the ratio of Ti/O close to the stoichiometric revealed formation of oxide. The same molar ratio has also been obtained from the EDS analysis of the samples. Generally, there is no observable change in the peak intensities of Ti as a function of Sr dopant concentration. However, the peak intensities of the Sr 3d are shown to increase with increasing the Sr dopant concentration, in great agreement with the EDS data.

To investigate the optical properties of the fabricated electrodes, the diffuse reflectance spectra (DRS) of the annealed Sr-doped nanotube arrays were measured; see Figure 5.

In general, the absorption edge of the material shows a red shift with increasing the dopant concentration. Also, the pH of the electrolyte used during the fabrication, at the same $Sr(OH)_2$ concentration, seems to affect the light absorption capability of the material. For example, for electrodes fabricated at pH 2, increasing the dopant concentration resulted in a red shift in the absorption edge from 377 to 379 nm at a 0.04 M dopant concentration and reaches the maximum value of 402 nm at the highest dopant concentration (0.06 M). When the pH is changed to 3, increasing the dopant concentration resulted in a slight enhancement in the corresponding absorption edge values in samples with 0.02 and 0.04 M dopant concentrations. However, this trend was not observed for the sample fabricated in an electrolyte containing 0.06 M $Sr(OH)_2$ as the absorption edge of the electrode appears at a slightly lower value (400 nm) compared with that of 402 nm for the same electrode fabricated at pH 2. The overall trend observed in all samples can be attributed to the relation between processing parameters and the morphological and electrochemical properties of the synthesized nanotubes; see Table 1. Consequently, the DRS UV−vis spectra suggest that the Sr-doped nanotube electrodes might exhibit a higher solar light response than the undoped ones.

Figure 6a shows the photocurrent density (i_{ph}) versus applied potential obtained for the fabricated Sr-doped TiO_2 nanotube electrodes in 1.0 M KOH solution under AM 1.5 G (100 mW/cm^2) illumination. We chose the samples fabricated in solutions of pH 3 because they showed higher dopant concentrations (see Table 1) compared with those fabricated in solutions of pH 2. In general, the photocurrent increases with increasing the Sr-doping concentration. Note that the dark current density in all cases is approximately 5 μA/cm^2. The highest photocurrent (~1 mA/cm^2) was obtained for the electrode fabricated in electrolyte containing 0.06 M $Sr(OH)_2$. This sample also shows the highest negative shift in the photocurrent onset potential (−0.803 $V_{Ag/AgCl}$). In fact, the trend observed in increasing the photocurrent with Sr dopant concentration is analogous to that of the shift in the absorption edge discussed earlier.

The corresponding electrode photoconversion efficiency (η) was calculated using eq 1[1,11]

$$\eta\ (\%) = [(\text{total power output} - \text{electrical power input})/\text{light power input}] \times 100 = j_p[(1.23 - |E_{measured} - E_{ocp}|)/I_0] \times 100 \quad (1)$$

where j_p is the photocurrent density (mA cm^{-2}), $E_{measured}$ is the electrode potential (versus Ag/AgCl) of the working electrode at which the photocurrent was measured under illumination, E_{ocp} is the open-circuit potential, and I_0 is the intensity of the incident light (mW cm^{-2}). Figure 6b shows the three-electrode photoconversion efficiency (η) of the fabricated electrodes. The pure TiO_2 nanotube electrode (1.2 μm long) showed a very low η

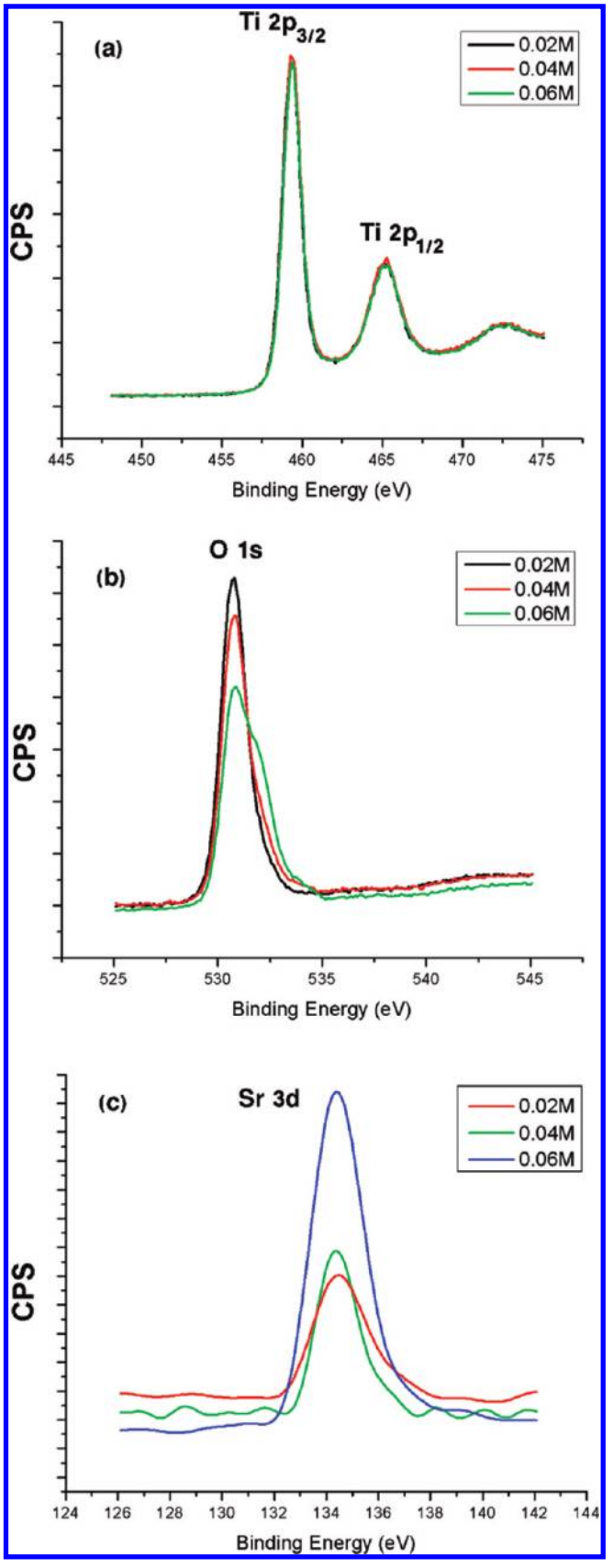

Figure 4. XPS spectra for as-prepared Sr-doped-TiO_2 nanotube samples showing (a) Ti 2p, (b) O 1s, and (c) Sr 3d as a function of Sr-dopant concentration.

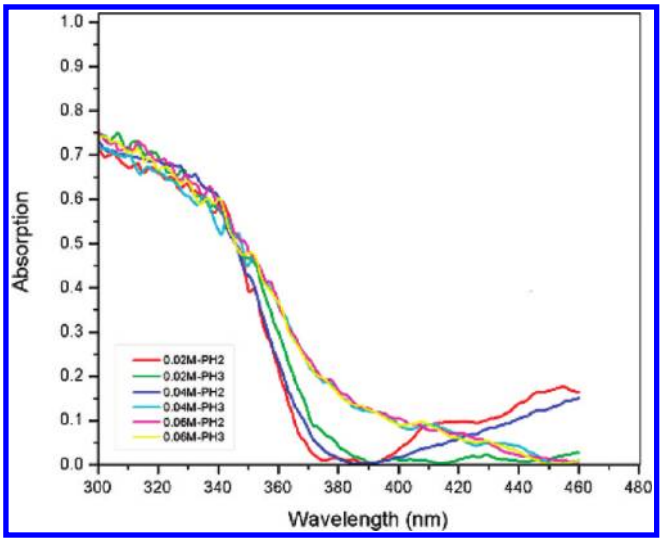

Figure 5. Variation of the DRS UV−vis spectra of Sr-doped TiO_2 nanotube samples with different Sr-dopant concentrations.

Table 1. Summary of the Properties of the Fabricated Sr-Doped TiO_2 Nanotubes

processing parameters		properties		
Sr(OH), M	pH	[Sr]-doped (%) from EDS[a]	average tube length (μm)	abs. edge ($\pm$2 nm)
0.02	2	0.05	0.7	377
	3	0.19	1.4	382
0.04	2	0.23	0.5	379
	3	0.28	1.0	399
0.06	2	0.36	1.1	402
	3	0.41	1.4	400

[a] The EDS data were taken over at least three different locations on each electrode with very reproducible results for the estimated amount of Sr; see Figure 1.

of about 0.2%. However, the highest η of 0.69% was recorded for the sample fabricated in an electrolyte containing 0.06 M $Sr(OH)_2$. The enhancement in η for the doped nanotube electrodes can be related, in part, to the effect of doping as the formation of $SrTiO_3$ (as confirmed by GAXRD) was shown to enhance the photoelectrochemical properties due to the strong band bending at the doped electrode surface compared to the undoped one.[31] The differences in η among all doped samples can also be related to the difference in the Sr amount doped into the TiO_2 matrix, the crystallinity as well as the nanotube length. Longer NTs have larger surface areas, enabling more light harvesting and larger active sites accessible to reactants in the aqueous environment. These factors lead to a higher efficiency, which is strongly in agreement with the results of Sulaeman and co-workers where i_{ph} activity under visible light irradiation is enhanced by designing strontium titanate with a high Sr/Ti atomic ratio.[32] The highest peak energy conversion efficiencies reported to date have been 0.60% or less over the whole solar spectrum;[1] thus, the obtained electrode efficiency of 0.69% for Sr-doped TiO_2 nanotubes in this work shows promising improvement toward a higher electrode efficiency.

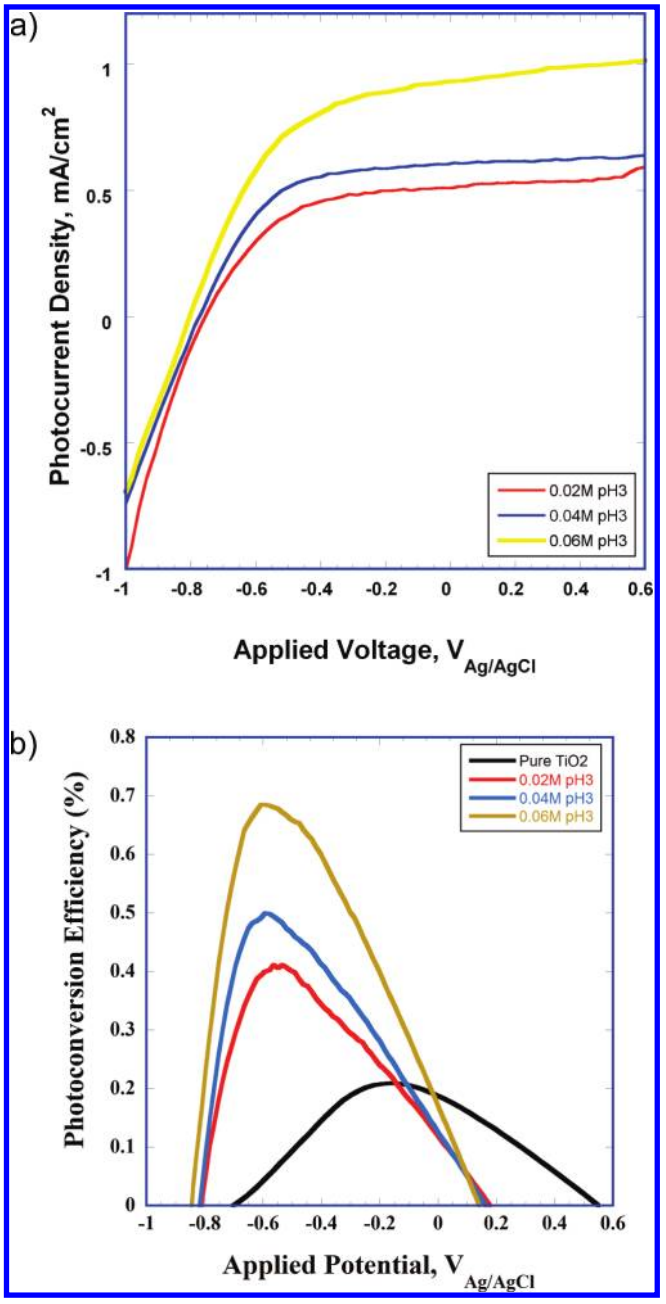

Figure 6. (a) Photocurrent density versus potential in 1 M KOH solution under AM 1.5 G illumination (100 mW/cm^2) for the Sr-doped TiO_2 nanotube electrodes fabricated at pH = 3. (b) Electrode photoconversion efficiency versus voltage characteristics for pure and Sr-doped TiO_2 nanotube electrodes fabricated at pH 3.

SUMMARY AND CONCLUSIONS

This work reports on the room-temperature electrochemical fabrication of highly ordered Sr-doped TiO_2 nanotube arrays and the investigation of their photoelectrochemical properties. Characterization of the as-prepared electrodes indicated that dopant concentration, up to the solubility limit of $Sr(OH)_2$, and pH of the electrolyte significantly influenced the morphology and quality of the fabricated electrodes. It is revealed that Sr doping of TiO_2 nanotubes resulted in a red shift in the absorption edge of the material to as long as 402 nm. Photoelectrochemical measurements revealed that Sr doping also improves the electrode photoconversion efficiency from 0.2% for the undoped electrode to 0.69% for the doped electrode. The obtained electrode efficiency of Sr-doped nanotubes of 0.69% is by far among the highest reported values in the literature for TiO_2-based photoelectrochemical cells.

AUTHOR INFORMATION

Corresponding Author

*E-mail: nkallam@mit.edu (N.K.A.), melsayed@gatech.edu (M.A.E.).

ACKNOWLEDGMENT

H.A.H. would like to acknowledge the financial support from Pacific Northwest National Laboratory. M.A.E. and N.K.A. would also like to thank the Department of Energy (DE-FG02-97ER14799) and the RAK-CAM Foundation for the support of this work.

REFERENCES

(1) Grimes, C. A.; Varghese, O. K.; Ranjan, S. *Light, Water, Hydrogen: The Solar Generation of Hydrogen by Water Photoelectrolysis*; Springer: Norwell, MA, 2007.
(2) Rao, C. N. R.; Raveau, B. *Transition Metal Oxides: Structure, Properties, and Synthesis of Ceramic Oxides*, 2nd ed.; Wiley-Interscience: New York, 1998.
(3) Allam, N. K.; El-Sayed, M. A. *J. Phys. Chem. C* **2010**, *114*, 12024–12029.
(4) Allam, N. K.; Grimes, C. A. *Sol. Energy Mater. Sol. Cells* **2008**, *92*, 1468–75.
(5) Allam, N. K. *Anodically Fabricated Metal Oxide Nanotube Arrays: A Useful Structure for Efficient Solar Energy Conversion*; VDM Verlag Dr. Müller: Berlin, 2011.
(6) Rettew, R. E.; Allam, N. K.; Alamgir, F. M. *ACS Appl. Mater. Interfaces* **2011**, *3*, 147–151.
(7) Allam, N. K.; Grimes, C. A. *Mater. Lett.* **2011**, *65*, 1949–1955.
(8) Hesabi, Z. R.; Allam, N. K.; Dahmen, K.; Garmestani, H.; El-Sayed, M. A. *ACS Appl. Mater. Interfaces* **2011**, *3*, 952–955.
(9) Allam, N. K.; Feng, X. J.; Grimes, C. A. *Chem. Mater.* **2008**, *20*, 6477–6481.
(10) Allam, N. K.; Alamgir, F.; El-Sayed, M. A. *ACS Nano* **2010**, *4*, 5819–5826.
(11) Grimes, C. A.; Mor, G. K. *TiO_2 Nanotube Arrays: Synthesis, Properties, and Applications*; Springer: Dordrecht, 2009.
(12) Bard, A. J.; Faulkner, L. R. *Electrochemical Methods: Fundamentals and Applications*, 2nd ed.; John Wiley & Sons: New York, 2001.
(13) Deng, L.; Wang, S.; Liu, D.; Zhu, B.; Huang, W.; Wu, S.; Zhang, S. *Catal. Lett.* **2009**, *129*, 513.
(14) Kapoor, P. N.; Uma, S.; Rodriguez, S.; Klabunde, K. J. *J. Mol. Catal. A* **2005**, *229*, 145.
(15) Allam, N. K.; Shankar, K.; Grimes, C. A. *J. Mater. Chem.* **2008**, *18*, 2341.
(16) Park, J. H.; Kim, S.; Bard, A. J. *Nano Lett.* **2006**, *6*, 25.
(17) Tokudome, H.; Miyauchi, M. *Chem. Lett.* **2004**, *33*, 1108.
(18) Kumar, A.; Santangelo, P. G.; Lewis, N. S. *J. Phys. Chem.* **1992**, *96*, 834.
(19) Liu, Y.; Xie, L.; Li, Y.; Yang, R.; Qu, J.; Li, Y.; Li, X. *J. Power Sources* **2008**, *183*, 701.
(20) Ueda, M.; Otsuka-Yao-Matsuo, S. *Sci. Technol. Adv. Mater.* **2003**, *5*, 187.
(21) Zhang, J.; Bang, J. H.; Tang, C.; Kamat, P. V. *ACS Nano* **2010**, *4*, 387.
(22) Zhang, J.; Tang, C.; Bang, J. H. *Electrochem. Commun.* **2010**, *12*, 1124.

(23) Zhang, X.; Huo, K.; Hu, L.; Wu, Z.; Chuw, P. K. *J. Am. Ceram. Soc.* **2010**, *93*, 2771.
(24) Jitputti, J.; Charoensirithavorn, P.; Yoshikawa, S. *Chem. Lett.* **2007**, *36*, 1508.
(25) Macdonald, D. D. *J. Electrochem. Soc.* **1993**, *140*, L27–L30.
(26) Patnaik, P. *Handbook of Inorganic Chemicals*; The McGraw-Hill Companies, Inc.: New York, 2002.
(27) Neretina, S.; Hughes, R. A.; Devenyi, G. A.; Sochinskii, N. V.; Preston, J. S.; Mascher, P. *Appl. Surf. Sci.* **2009**, *255*, 5674.
(28) Li, Y.; Gao, X. P.; Li, G. R.; Pan, G. L.; Yan, T. Y.; Zhu, H. Y. *J. Phys. Chem. C* **2009**, *113*, 4386.
(29) Gaft, M.; Reisfeld, R.; Panczer, G. Luminescent Minerals. In *Modern Luminescence Spectroscopy of Minerals and Materials*; Springer: Berlin, 2005; p 45.
(30) Zhang, W.; Shen, Y.; Pan, H.; Lin, K.; Liu, X.; Darvell, B. W.; Lu, W. W.; Chang, J.; Deng, L.; Wang, D.; Huang, W. *Acta Biomater.* **2010**, *7*, 800.
(31) Mavroides, J. G.; Kafalas, J. A.; Kolesar, D. F. *Appl. Phys. Lett.* **1976**, *28*, 241.
(32) Sulaeman, U.; Yin, S.; Sato, T. *Appl. Phys. Lett.* **2010**, *97*, 103102.